Applied Catalysis B: Environmental 121–122 (2012) 115–122

Contents lists available at SciVerse ScienceDirect

Applied Catalysis B: Environmental

journal homepage: www.elsevier.com/locate/apcatb

Chloride-free Cu-modified SAPO-37 catalyst for the oxidative carbonylation of methanol in the gas phase

Thi Thuy Hanh Dang, Michael Bartoszek, Matthias Schneider, Dang-Lanh Hoang, Ursula Bentrup, Andreas Martin*

Leibniz-Institut für Katalyse e.V. an der Universität Rostock, Albert-Einstein-Str. 29a, D-18059 Rostock, Germany

ARTICLE INFO

Article history:
Received 21 December 2011
Received in revised form 22 March 2012
Accepted 27 March 2012
Available online 4 April 2012

Keywords:
SAPO-37
Cu-modified SAPO-37
Dimethyl carbonate
Oxidative carbonylation of methanol
Solid state ion exchange

ABSTRACT

The substitution of harmful phosgene or chloride-containing catalysts in the synthesis of dimethyl carbonate (DMC) and its use as "green solvent" or polycarbonate building block direct its manufacture towards environmental benign syntheses. Thus, copper was introduced into silicoaluminophosphate structure SAPO-37 (belonging to the same FAU structure family like aluminosilicate zeolites Y and X) by solid state ion exchange (SSIE) using Cu(II) acetyl acetonate. This strategy circumvented structural breakdown being observed when using aqueous copper solutions for impregnation or ion exchange. The SSIE efficiently ran when the organic template is widely extracted from the synthesis form of SAPO-37, e.g. through treatment with methanolic HCl. The parent SAPO-37, template-free SAPO-37 and Cu-SAPO-37 materials were characterized by XRD, TG, temperature programmed reduction (TPR), temperature programmed desorption of ammonia (TPDA) and FTIR spectroscopy of adsorbed pyridine and CO. The Cu-SAPO-37 catalyst pre-treated in inert gas exhibits a high selectivity for DMC and dimethoxymethane (DMM) in the oxidative carbonylation of methanol (OCM). The catalytic behavior of Cu-SAPO-37 is shown to be comparable with those of a Cu-containing Y zeolite catalyst that is so far regarded as one of the best chloride-free catalyst for the OCM reaction in the gas phase.

1. Introduction

Feed mixtures composed of alcohols, carbon monoxide and oxygen can be catalytically transformed into dialkyl carbonates. The interest in eco-friendly manufacturing of organic carbonates is high due to the prohibition and restriction of phosgene use, respectively, and to their growing demand being useful as raw materials for polycarbonates and polyurethanes, electrolyte solvents for lithium ion batteries, organic solvents, fuel additives, and green reagents [1]. In particular, dimethyl carbonate (DMC) the simplest homologue of organic carbonates is a reasonable synthetic target if CO_2 could directly be used for the reaction with methanol (MeOH) [2]. But, as long as the unfavorable thermodynamics of this process [3] limits economic product yields, DMC synthesis from the oxidative carbonylation of methanol (OCM) will be an alternative. OCM catalyzed by cuprous chloride in a slurry phase reaction is commercialized by EniChem S.p.A, although hydrolysis of CuCl and concomitant activity loss requires co-feeding of HCl that imposes corrosion and environmental problems [4]. Gas phase OCM on CuCl supported on alumosilicate zeolites or mesoporous MCM-41 [5] is possible, but space–time–yields (STY) in continuous flow processes are low, 2–3 $g_{DMC}/(dm_{cat}{}^3\,h)$ in the latter case. In addition, the drawback of using chloride-containing solids is not solved.

Chloride-free Cu modified zeolite Y is reported to allow STY of more than 500 $g_{DMC}/(dm_{cat}{}^3\,h)$ at a methanol conversion of 5–15% [6]. However, the Cu content has to be high enough to avoid any Brønsted acidity which would cause undesired conversion of methanol to dimethyl ether (DME) occurring on residual acid sites after Cu modification.

Within the family of aluminophosphates, AlPO-37 belongs to the same FAU structure type as zeolites X and Y [7], but has no Brønsted acid sites at all due to elemental composition and thus, structural reasons. Introduction of Si into aluminophosphates during the synthesis to replace P in the crystalline framework would result in SAPO materials that possesses Brønsted acid sites, but of modified strength in comparison to zeolite Y [8,9]. The use of SAPO-37 in acid-catalyzed reactions is described, e.g. for o-xylene isomerisation [10], reaction of cyclohexene with H_2O_2 [11], isobutene/2-butene alkylation [12], cracking of *n*-heptane and 2,2,4-trimethylpentane [13] as well as the conversion of *n*-hexane, cyclohexane and gas oil [14]. Because of structural degradation of non-modified, Brønsted-acid SAPO-37 in the presence of water vapor traces, applications in oxidation reactions are rare. Likewise, modification of the parent SAPO-37 by copper through impregnation with aqueous solution would inevitably destroy the structure. This may be the reason why

* Corresponding author. Tel.: +49 381 1281 246; fax: +49 381 1281 51246.
E-mail address: andreas.martin@catalysis.de (A. Martin).
URL: http://www.catalysis.de/ (A. Martin).

0926-3373/$ – see front matter © 2012 Elsevier B.V. All rights reserved.
http://dx.doi.org/10.1016/j.apcatb.2012.03.031

SAPO-37 used as carrier for catalytically active copper to catalyze the OCM reaction has not been reported so far.

We present in this paper the first successful non-aqueous modification of SAPO-37 with Cu and the use of Cu-containing SAPO-37 as catalyst in the gas phase OCM reaction to DMC. For preparing the catalyst, the synthesis of stable Cu-free SAPO-37 was carried out by the method reported by Malla and Komarneni [15], in which a methanolic HCl solution was used for template removal. It was pointed out [15] that, for the synthesis of stable SAPO-37, the two template compounds (tetramethylammonium hydroxide (TMAOH) and tetrapropylammonium hydroxide (TPAOH)) are necessary. The templates occupy different subunits within the FAU structure of SAPO-37, viz. TMA^+ the sodalite cages and the bulkier TPA^+ the super cages. Treatment of the synthesis form of SAPO-37 with methanolic HCl can remove the TPA^+ but not TMA^+. The remaining TMA^+ ions seem to stabilize the crystal structure against degradation by water. The modification of a SAPO-37 sample treated this way with Cu was carried out by using solid Cu(II) acetyl acetonate ($Cu(acac)_2$). This bases upon the principles of solid state ion exchange (SSIE) [16] subjecting the mixed SAPO-37 and $Cu(acac)_2$ to an inert atmosphere at higher temperature. The as-synthesized SAPO-37, the extracted SAPO-37 and the Cu-SAPO-37 materials were characterized by X-ray diffraction (XRD), temperature-programmed desorption of ammonia (TPDA), temperature-programmed reduction (TPR) as well as FTIR spectroscopy of adsorbed pyridine and CO. The OCM reaction was performed on calcined (550 °C, air, 6 h) and further activated (650 °C, argon, 6 h) Cu-SAPO-37 catalysts in a flow reactor under normal pressure as well as under a pressure of 0.4 MPa in the temperature ranges from 120 to 220 °C and 120 to 180 °C, respectively.

2. Experimental

2.1. SAPO-37 synthesis

Pseudo-boehmite Catapal B (Sasol North America Inc.), orthophosphoric acid (85%, Acros Organics), hydrophilic fumed silica Aerosil 200 (Evonik Industries AG), TPAOH (40% in water, Merck) and TMAOH (25% in water, Merck) were chosen as the source materials for SAPO-37 synthesis. Synthesis gels were prepared using procedures previously described [10]. The gel composition (molar basis) was 1 Al_2O_3:1 P_2O_5:0.4 SiO_2:1 $(TPA)_2O$:0.025 $(TMA)_2O$. In parallel steps, the pseudo-boehmite was digested by phosphoric acid under stirring, and silica was immersed into a mixture of both templates keeping the template ratio $(TPA)_2O$:$(TMA)_2O$ constant at 40. Then, the solutions were mixed under continuous stirring. The resulting gel was transferred into a Teflon-lined autoclave which was sealed and heated in an oven under static conditions at autogenous pressure to 200 °C. It turned out in preliminary syntheses that there exists a slot in the crystallization time deciding on the phase purity. Phase-pure as-synthesized SAPO-37 (denoted as SAPO-37-as) resulted after 20 h crystallization time; AlPO-5 and/or SAPO-5 alien phases occurred not until increased crystallization time, i.e. ca. 24 h. According to these preceding results, the crystallization time was set to 20 h, in general.

The synthesis product was recovered by filtration and then washed with de-ionized water followed by drying in ambient air.

2.2. Template extraction

The template extraction with methanolic HCl followed the procedure described in [15] with slight modification. A sample amount of 0.5 g SAPO-37-as was immersed in 25 ml methanolic HCl (1.0 M) solution. The resulting slurry was put into a Teflon-lined autoclave (100 ml capacity) and kept at 150 °C for 16 h. After recovering by filtration, the sample was dried at 60 °C. This template extracted sample is denoted as SAPO-37-ex in the following.

2.3. Cu modification of SAPO-37

Attempts to introduce Cu by ion exchange into the synthesis form of SAPO-37 according to the suggestion of Zamadics and Kevan [17] failed. Because a direct exchange seemed to be hardly possible, the procedure comprised in a first stage the exchange of the template (assumed to be fixed to the interior of the FAU structure in form of $(C_3H_7)_4N^+$) by NH_4^+ using a NH_4NO_3 solution (stirring at room temperature (r.t.) for 14 h), and in a second stage the impregnation of the dried NH_4^+ form by a $Cu(NO_3)_2$ solution (1 M, 80 °C, 1 h). XRD patterns, not shown here, had actually revealed far-going destruction of crystallinity after completion of this treatment.

To avoid contact with aqueous solution(s), the SAPO-37-ex sample was mixed with an appropriate amount of $Cu(acac)_2$ powder corresponding to a Cu/acid site ratio of ca. 1. $Cu(acac)_2$ has a melting point of 245 °C and a boiling point of 263 °C (under decomposition). The principal product of the thermal decomposition of $Cu(acac)_2$ is acetyl acetone over the entire temperature range [18]. Decomposition of $Cu(acac)_2$ in the presence of H_2O and N_2 yields copper nanoparticles, where the reduction of Cu^{2+} to Cu^0 should occur at the expense of ligand oxidation [19]. In the presence of O_2, however, Cu_2O is found at low O_2 pressure and CuO at higher O_2 concentration [20].

The physical mixture of SAPO-37-ex sample and $Cu(acac)_2$ powder was (i) calcined at 550 °C in air for 6 h and (ii) followed by an inert treatment in a flow of pure argon (50 ml/min, Ar purity grade 5.5, Air Liquide) at 650 °C for further 6 h to promote a SSIE of protonic sites by copper cations. Referring to previous works of Richter et al. [6] this second pre-treatment will be denoted below as activation. The solids received were denoted as Cu-SAPO-37-ex. The copper content amounted to 11.5 wt.% as determined by AAS. CHN analysis was performed to get information on residual template. The sample contained 0.05 wt.% C, 0.12 wt.% N and 0.34 wt.% H. Because methanolic HCl was used for template extraction, the Cl^- content of the sample Cu-SAPO-37-ex was checked by potentiometric titration. It could be shown that no chlorine was left over in the solid.

2.4. Catalyst characterization

The structure and crystallinity of as-synthesized samples as well as samples at various stages of post-treatment and Cu modification were examined by XRD using a transmission diffractometer (STOE) with CuKα1 radiation and recording of the pattern with a position sensitive detector (PSD) in the 2θ range from 2° to 60°.

Surface areas and pore volumes were determined by nitrogen adsorption at −196 °C applying the ASAP 2010 characterization unit (Micromeritics). Samples were measured after preceding in situ template removal carried out by evacuation to 0.13 Pa and stepwise increase of the temperature up to 450 °C (heating ramp: 0.5 K/min) and holding for 12 h.

Thermoanalysis (TG/DSC) was carried out on a Sensys TG–DSC (Setaram). Samples of ca. 50 mg were heated in flowing air up to 830 °C at a heating rate of 5 K/min where Al_2O_3 was chosen as reference material.

The copper content of the samples was determined by atomic absorption spectroscopy (AAS) using an Analyst 300 device (Perkin Elmer). CHN analysis was carried out using a CHNS microanalyser Truspec (Leco).

TPDA of Cu-free SAPO-37-ex sample was carried out in a home-made apparatus consisting of a gas flow system, a high-temperature oven and a quartz reactor. Desorption of NH_3 was monitored and evaluated by a thermal conductivity detector, TCD

(GOW-Mac Instrument Co.), which was calibrated by performing thermal decomposition of varying amounts of manganese ammonium phosphate. A special procedure was recently developed in our lab for determining the acidity of SAPO-37-ex samples. The TPDA runs in this case in parallel to further template removal due to thermal treatment. The procedure comprised the following steps in sequence. (i) A dried SAPO-37-ex sample was placed into the reactor of the TPDA apparatus and pre-treated in a flow of He (50 ml/min) at 160 °C for 0.5 h to eliminate any traces of water. This was followed by a new calcination at 400 °C (He) for further 0.5 h. In this condition, template should still exist in the pore system, or according to [15], in sodalite cages. (ii) After cooling the sample in He flow from 400 °C down to 100 °C, NH_3 adsorption was carried out at 100 °C until saturation (10 vol.% NH_3, 20 ml/min). This was followed by flushing of the whole system before the TPDA was started running from 100 °C to 400 °C with a heating rate of 10 K/min. The step (ii) was repeated three times (designed as TPDA1, TPDA2 and TPDA3) for verifying the concomitant release excess template, if present. (iii) After the last TPDA run, the sample was annealed at 550 °C (He) for further 0.5 h. According to the TGA measurements, this completely eliminates the rest of template. (iv) After cooling down the sample in He flow to 100 °C, the NH_3 adsorption and following TPDA were carried out as described in the step 2, but up to 550 °C. This step was repeated three times, as well. The measurements are designed as TPDA4, TPDA5 and TPDA6.

TPR was carried out in the same home-made apparatus used for TPDA. The material was calcined once more in situ at 400 °C in an air flow for 0.5 h and then cooled down to 50 °C in a dried nitrogen flow. Afterwards, the TPR run was carried out from 50 to 550 °C in a 5.03 vol.% H_2 containing argon flow at a heating rate of 10 K/min. Optimum sample weights corresponding to a reduction with gas flow rate of 15 ml/min had been estimated according to the equation proposed by Monti and Baiker [21]. The quantitative analysis of the TPR results, based on the integration of calibrated hydrogen consumption peak areas, was carried out by the method described elsewhere [22].

FTIR measurements in transmission were carried out on a Bruker Tensor 27 spectrometer using self-supporting wafers. A heatable homemade reaction cell with CaF_2 windows was used. The cell was connected to a gas-dosing and evacuation system, respectively. The sample powders were pressed into self-supporting discs with a diameter of 20 mm and a weight of 50 mg. For acidity characterization pyridine was used as probe molecule. Before pyridine adsorption, the samples were pretreated by heating in synthetic air up to 400 °C for 30 min and cooling down to r.t. Pyridine was adsorbed at r.t. until saturation. The physisorbed pyridine was removed by flushing with He. Then, the pyridine desorption was followed by heating the sample again in He stream up to 400 °C and recording spectra every 50 °C.

The adsorption of CO was carried out at r.t. after pre-treating both the Cu-SAPO-37-ex samples in air (calcined sample) and He (activated sample) at 400 °C for 30 min, respectively. Generally, difference spectra were evaluated, obtained by subtracting the respective spectrum of the pre-treated sample from the adsorbate spectrum.

2.5. Catalytic tests

2.5.1. Test at normal pressure

The gas phase OCM was carried out in a flow type quartz micro-reactor of an Autochem 2910 (Micromeritics) equipment. Liquid methanol was injected into the gas feed by a syringe pump (Harvard Instruments). A heated quartz tube was used as an evaporator. At least a feed gas composition of 5.8 vol.% CO, 2.9 vol.% O_2, 2.2 vol.% Ar, 80.4 vol.% He (all from Air Liquide) and 8.7 vol.% MeOH was achieved. The total flow rate amounted to 54.8 cm^3/min. With a catalyst sample amount of 0.1 g, this results in a space velocity of 16,440 h^{-1} (assuming an average apparent density of this type of catalysts of 0.5 g/cm^3). Product analysis was accomplished by an on-line coupled mass spectrometer (Omnistar, Pfeiffer-Vacuum). Further product identification was performed off-line with a GC–MS system (MD800, Thermo Instruments). The temperature-programmed catalytic runs started with an isothermal period at 120 °C for 30 min followed by a linear heating of the catalyst under feed up to a maximum reaction temperature of 220 °C with a ramp of 1 K/min.

An in situ pre-treatment of the catalyst preceded each run, consisting of a temperature programmed annealing up to 160 °C (heating rate: 5 K/min) with isothermal hold for 30 min to remove adsorbed water, cooling down the sample in a He flow to 120 °C, and starting the experiment by switching from He to feed. The methanol conversion was calculated from the amount of products formed, considering the stoichiometry (for details, see e.g. [6,23]). Product selectivity referred to the sum of dimethyl carbonate (DMC), dimethoxymethane (DMM), methyl formate (MF), and dimethyl ether (DME).

2.5.2. Test under pressure (0.4 MPa)

Catalytic measurements under pressure were performed in a temperature range of 130–170 °C using a reaction system consisted of a stainless steel flow micro-reactor and gas supply equipments described in detail in [24]. 1.0 g of catalyst sample (0.3–0.7 mm particle size), diluted by 0.5 g of graphite for isothermal process control, was used. The composition (in vol.%) of the gas reactant mixture consisted of MeOH, CO, O_2 and N_2 was 20.0, 40.0, 1.3 and 38.7, respectively. The products of the OCM reaction were analyzed on-line by using a gas chromatograph HP 5890 (Agilent Technologies), equipped with a flame ionization detector (FID) and a capillary column HP-Plot/Q (30 m × 0.53 mm × 40 μm). The methanol conversion and the selectivity of products were calculated as described above.

3. Results and discussion

3.1. Catalyst characterization

Fig. 1 reveals the XRD patterns of SAPO-37 materials: (a) SAPO-37-as, (b) SAPO-37-as, calcined at 440 °C, followed by rehydration, (c) SAPO-37-ex and (d) SAPO-37-ex, annealed at 160 °C, followed by rehydration. The rehydration was carried out by keeping the sample in moisturized air for 24 h. As shown, the crystallinity of SAPO-37-as is strongly deteriorated after calcination at 440 °C

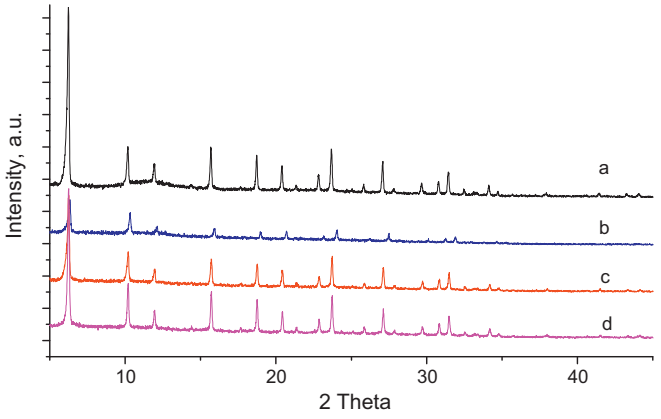

Fig. 1. XRD patterns of the obtained SAPO-37 materials: (a) SAPO-37-as, (b) SAPO-37-as, calcined at 440 °C, followed by rehydration, (c) SAPO-37-ex and (d) SAPO-37-ex, annealed at 160 °C, followed by rehydration.

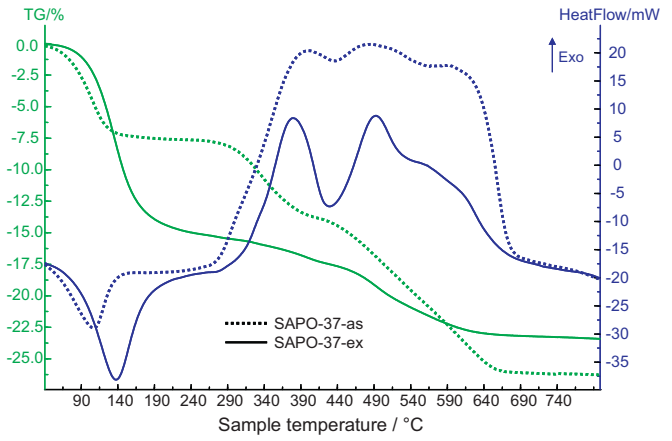

Fig. 2. TG–DTA analysis of SAPO-37-as and SAPO-37-ex.

followed by rehydration (sample (b)). The further XRD measurements, not shown here, demonstrated that the higher the temperature the more templates were removed. This could be proven by N_2 adsorption at −196 °C [24] showing a drastic development of BET specific surface area from 22 m^2/g to ca. 930 m^2/g as the temperatures increases from 50 °C to 450 °C, respectively. However, similar to sample (b), a complete amorphization of the template-free SAPO-37 takes place sooner or later if it has contact with moisturized air. This amorphization is reasoned by the hydration process taking place at ≡P—O—Al≡ bounds [25]. Unlike this, the crystallinity of SAPO-37-ex, obtained after extraction using 1.0 M methanolic HCl solution (c), remains intact in a moisturized air after the annealing at 160 °C (d). It was revealed in [24] that this is the highest temperature at which the template stabilizing ≡P—O—Al≡ bounds is still in FAU cages and, therefore, impedes the deteriorating hydration.

Fig. 2 shows the results of TG–DTA analyses of SAPO-37-as and SAPO-37-ex samples. It can be observed that the weight loss occurred at least in three stages. The first (endothermic) stage, observed at temperatures ≤250 °C, can be assigned to desorption of water. The second stage at 250–450 °C and third stage at 440–650 °C may correlate with the removal of TPA^+ and TMA^+ from super cages and of TMA^+ from sodalite cages of the FAU structure, respectively [15]. The weight losses corresponding to each stage are summarized in Table 1. It appears that the water desorption drastically increases in case of SAPO-37-ex sample. This can be explained by taking into account that the extraction made a larger proportion of pores accessible for water adsorption. The lower weight losses at the second and third stages of the SAPO-37-ex reveal the efficiency of the templates extraction by methanolic HCl solution that has obviously removed a large proportion of the templates.

Some results of acidity characterization of SAPO-37-ex are shown in Fig. 3 and Table 2. In Fig. 3a, a two-peak desorption pattern of TPDA1-3 runs (family of profiles A) with T_{max} at 193 °C and 347 °C, respectively, is observed, pointing to the existence of weak and strong acid sites. The high-temperature (HT) shoulders centered at 347 °C reveal a relative high acid strength assignable to the existence of Brønsted acid sites as expected after successful incorporation of Si in tetrahedral framework positions of the FAU

Table 1
Thermogravimetric weight losses corresponding to each stage of TG–DTA analysis.

Pre-treatment	First stage (wt.%) <250 °C	Second stage (wt.%) 250–440 °C	Third stage (wt.%) 440–650 °C	Sum (wt.%)
SAPO-37-as	7.5	6.88	11.86	26.24
SAPO-37-ex	15.1	2.40	5.95	23.45

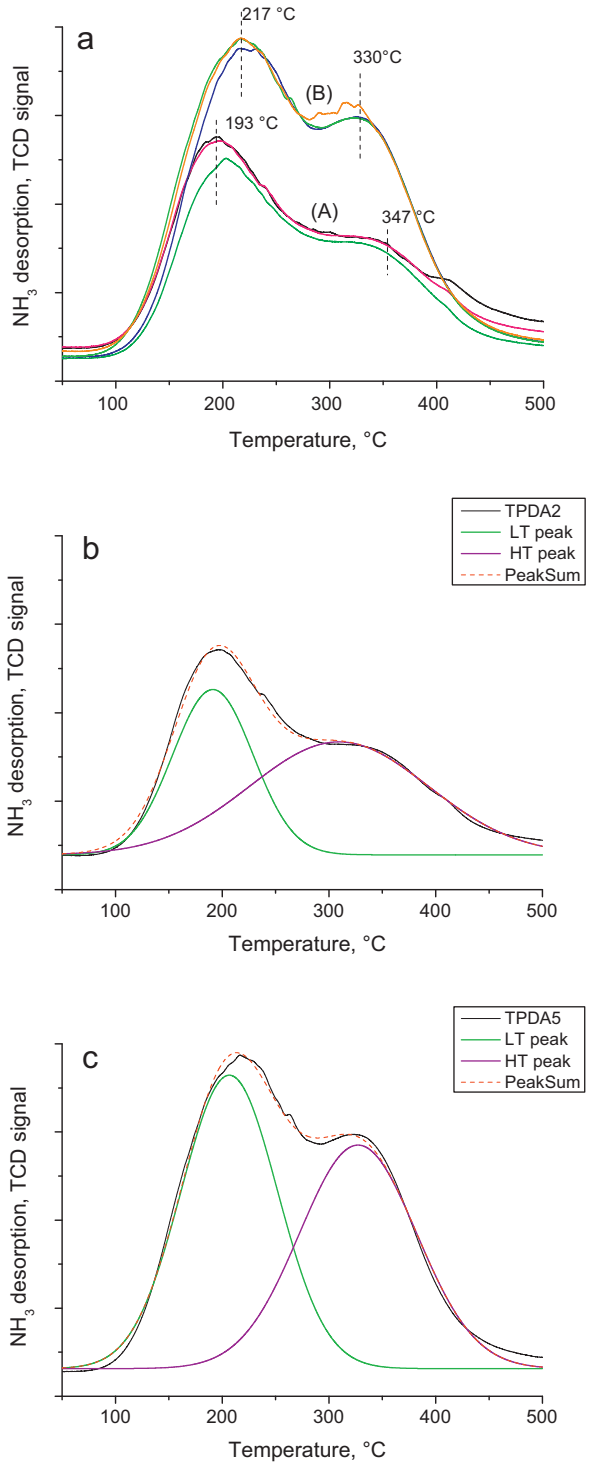

Fig. 3. TPDA1-3 (family A) and TPDA4-6 (family B) profiles of SAPO-37-ex (a), Gaussian fitting of TPD2 (b), Gaussian fitting of TPD5 (c).

structure substituting a part of P. This can be confirmed by FTIR-spectroscopic investigation of pyridine adsorption as discussed below. The amount of overall acid sites of the sample SAPO-37-ex, which was treated at 400 °C, was 1.45 mmol/g and the part of Brønsted acid sites 0.88 mmol/g when fitted by two Gaussian peaks (TPDA2). TPDA4-6 experiments (family of profiles B) show a similar desorption pattern consisting of two peaks with higher intensities at T_{max} = 217 °C and 330 °C. This hints on the effect of the high temperature treatment carried out at 550 °C after TPDA1-3 runs that

Table 2
Quantitative TPDA results obtained for SAPO-37-ex annealed at 160 °C.

	TPDA1	TPDA2	TPDA3	TPDA4	TPDA5	TPDA6
Total acidity (mmol NH_3/g)	1.51	1.45	1.45	2.51	2.53	2.59
Gaussian fitting						
LT peak						
Area (%)		39.70			52.00	
Acidity (mmol NH_3/g)		0.57			1.31	
HT peak						
Area (%)		60.30			48.00	
Acidity (mmol NH_3/g)		0.88			1.22	

eliminates further template components freeing more sites for NH_3 adsorption. The quantitative results presented in Table 2 confirm this idea, showing the increases of concentration of the total acidity and Brønsted acid sites to 2.53 mmol/g and 1 mmol/g (TPDA5), respectively. The TPDA2 and TPDA5 profiles fitted by the Gaussian function integrated in the software package Origin 8 (Origin Lab Corporation, USA) are displayed in Fig. 3b and c.

Fig. 4 summarizes the results of the XRD analysis of SAPO-37-ex (a) and Cu-SAPO-37-ex (calcined (b) and activated (c)). It can be seen that, like SAPO-37-ex, Cu-SAPO-37-ex prepared by SSIE exhibits the similar XRD pattern being characteristic for the FAU structure. In addition, crystalline CuO can be observed for both the calcined and activated Cu-SAPO-37-ex samples. But, the presence of crystalline Cu_2O portions cannot be revealed by XRD. Probably Cu_2O might be present but it cannot be seen by XRD due to its small content and/or high dispersion of these species. This seems to agree with TPR results presented below.

Fig. 5 shows the TPR profiles obtained for the calcined (a) and activated (b) Cu-SAPO-37-ex sample. The profile of the calcined sample exhibits a main intensive reduction peak at 286 °C. The total amount of hydrogen consumed is 1.35 mmol H_2/g. This corresponds to an oxidation state change of ca. 1.5, calculated from the total amount of hydrogen consumed [22,26]. This suggests a reduction of an initial mixture consisted of Cu^+ and Cu^{2+}, with Cu^{2+} as dominant species to a final mixture consisted of Cu^+ and Cu^0, with Cu^0 being predominant. The XRD measurement on the samples reduced by TPR (not shown here) confirms this behavior revealing the existence of Cu^0. Unlike this, the TPR profile of the activated sample consists of several peaks, some located at around 280 °C and another around 430 °C. The more complex TPR profile

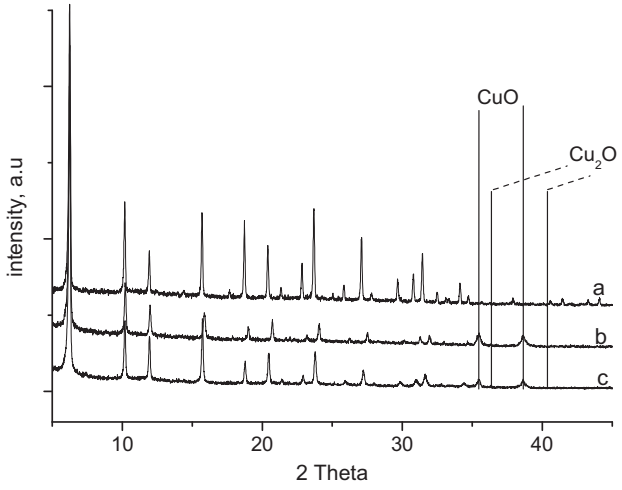

Fig. 4. XRD patterns of SAPO-37-ex (a) and Cu-SAPO-37-ex (calcined (b) and activated (c)).

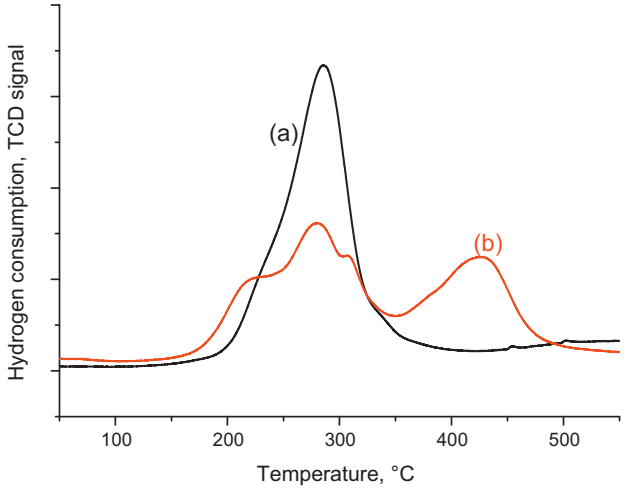

Fig. 5. TPR profiles of Cu-SAPO-37-ex (calcined (a) and activated (b)).

of the activated sample suggests that, during the activation, different Cu oxide types could be formed which varied in their locations on and/or in their interaction degree with the SAPO-37 matrix. This leads to different facilities of Cu oxide species against reduction. The total hydrogen consumption remains, however, almost unchanged at 1.34 mmol H_2/g, corresponding to an oxidation state change of 1.5 as well. These findings suggest that the activation does not strongly affect the oxidation states of Cu but radically changes the Cu distribution in the SAPO channels. The latter fact is partly confirmed by the results of CO adsorption, too. However, concerning changes of the oxidation state the results of CO adsorption studies lead to a different conclusion (vide infra).

The FTIR-spectroscopic investigation of pyridine adsorption is a widely used method for the characterization of both Brønsted and Lewis acidic sites [27–29]. The typical band of pyridine fixed to Brønsted acid sites (PyH^+) is observed at around 1540 cm^{-1}. Bands resulting from pyridine fixed to Lewis acid sites (L-Py) can be observed at around 1450 cm^{-1} and in the region 1625–1600 cm^{-1}. From the band position in the latter region the strength of Lewis acid sites can be evaluated [29].

The FTIR spectra of pyridine adsorbed at 150 °C on Cu-free SAPO-37-ex and the calcined as well as the activated Cu-SAPO-37-ex samples are shown in Fig. 6. Quantitative data are summarized in Table 3, where integral intensities of the characteristic bands at 1541 cm^{-1} (PyH^+) and 1451 cm^{-1} (L-Py) are given normalized to the BET surface area of the samples. As expected, SAPO-37-ex (Fig. 6a) possesses Brønsted acid sites indicating by the intensive band of PyH^+ cations at 1541 cm^{-1}. Only a slight intense L-Py band can be observed at 1451 cm^{-1} resulting from Al^{3+} Lewis sites of SAPO-37-ex.

The calcined sample Cu-SAPO-37-ex (Fig. 6b) reveals a distinct lower Brønsted acidity while at the activated sample (Fig. 6c) only a marginal Brønsted acidity remains. Otherwise, a drastic increase of the L-Py bands at 1451 cm^{-1} and 1607 cm^{-1} can be observed

Table 3
Integral intensities (arbitrary units) of FTIR pyridine absorption bands at 150 °C, normalized to the BET surface area.

Sample	S_{BET} (m^2/g)	Band intensities normalized ($\times 10^{-3}$)	
		PyH^+ (1541 cm^{-1})	L-Py (1451 cm^{-1})
SAPO-37-ex	924	10.84	0.68
Cu-SAPO-37-ex (calcined)	773	2.48	26.17
Cu-SAPO-37-ex (activated)	669	0.79	11.54

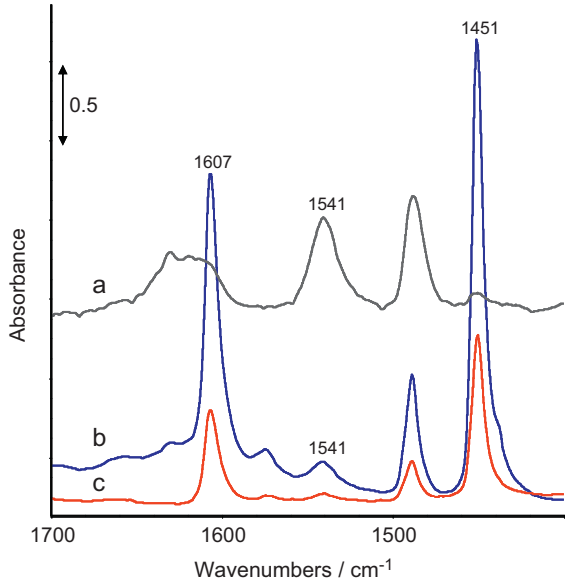

Fig. 6. Pyridine adsorbate FTIR spectra at 150 °C on SAPO-37-ex (a) and Cu-SAPO-35-ex (calcined (b) and activated (c)).

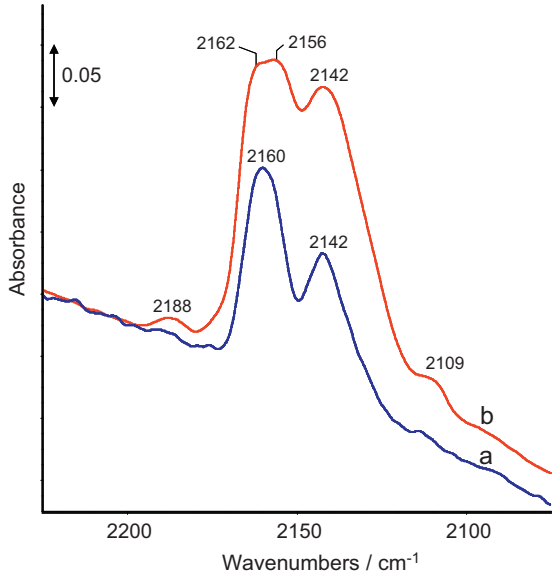

Fig. 7. FTIR spectra of CO adsorbed at room temperature on Cu-SAPO-35-ex (calcined (a) and activated (b)).

in both the Cu-SAPO-37-ex samples which result mainly from Cu^+ Lewis sites at definite positions in the SAPO-37 super cage [30]. These findings indicate the replacement of the acidic protons of SAPO-37-ex by Cu cations due to the SSIE.

Surprisingly, the spectrum of the activated sample (Fig. 6c) shows, compared to the spectrum of the calcined one (Fig. 6b), an overall low intensity. This is obviously due to a meanwhile rehydration of the sample and loss of crystallinity caused by a time interval between activating procedure and spectroscopic measurement. The different qualities of the spectra (not shown) obtained after pre-treatment of the respective wafers in the spectroscopic cell confirm this assumption.

Information concerning the presence and nature of Cu^+ cations is available from CO adsorbate spectra [31]. It is known from investigations of Cu-Y zeolites that depending on their position in the cages and their specific surroundings therein different positions of the Cu^+—CO bands have to be expected [31–33].

The obtained FTIR spectra of CO adsorbed on calcined and activated Cu-SAPO-37-ex are displayed in Fig. 7. The Cu^+—CO bands at 2160 cm^{-1} and 2142 cm^{-1} appear at similar positions as described for Cu-Y zeolite samples [30]. Both the bands indicate different locations of the Cu^+ cations in the super cage. Comparing the band intensities observed for the calcined and activated Cu-SAPO-37-ex samples distinct higher intensities were found for the activated sample resulting from an essential higher amount of Cu^+ species. Obviously, the activation procedure favors the autoreduction of Cu^{2+} cations to Cu^+ whereas the latter preferentially replace protonic sites as also demonstrated by the results of pyridine adsorption experiments.

The observed high frequency (HF) and low frequency (LF) bands indicate, like in the Cu-Y samples, different positions of the Cu^+ cations in the super cages of Cu-SAPO-37-ex. After activation the HF band becomes broader and is split into two components at 2162 and 2156 cm^{-1} which indicates the occupation of additional sites in the super cage by the Cu^+ cations. The low intensity band at

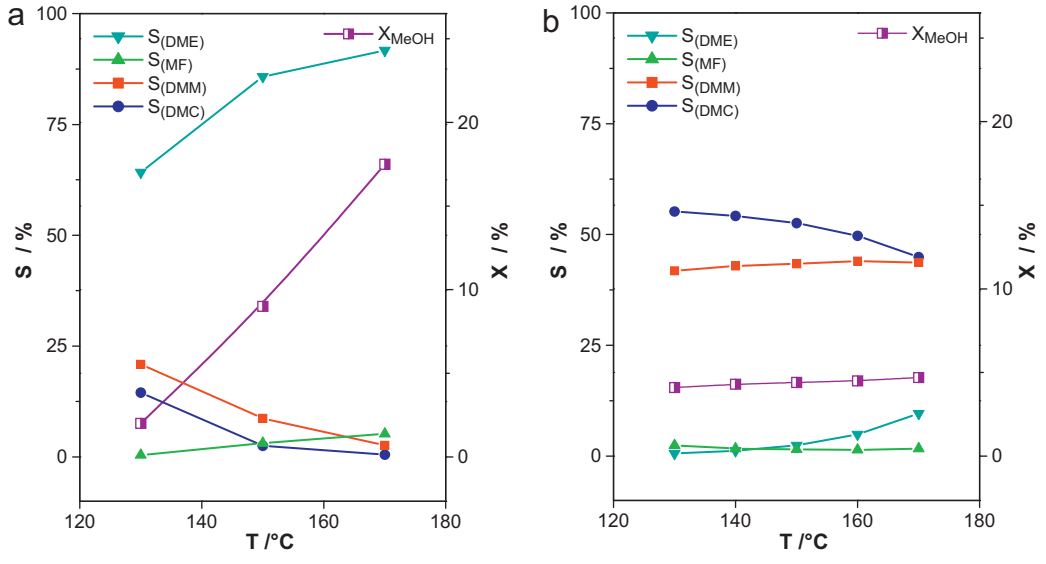

Fig. 8. Methanol conversion and product selectivities vs. reaction temperature obtained for calcined (a) and activated (b) Cu-SAPO-37-ex (0.4 MPa).

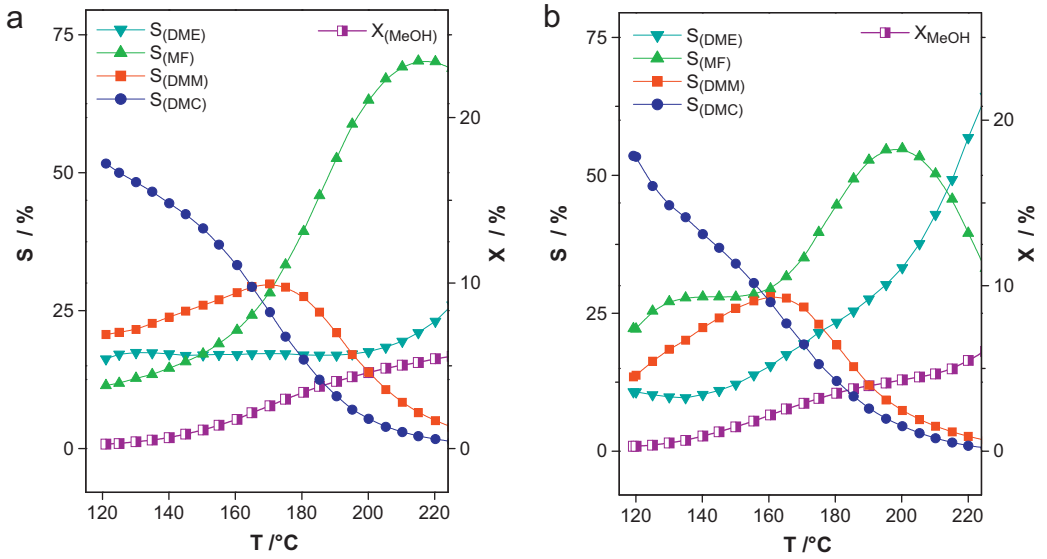

Fig. 9. Methanol conversion and product selectivities vs. reaction temperature obtained for Cu-SAPO-37-ex (a) and 16Cu-Y (b) under normal pressure. Both the samples were activated and contain 11.5 wt.% and 16.0 wt.% Cu, respectively.

2109 cm^{-1} was also observed on high loaded Cu-Y [30] and partly reduced CuO samples [34,35] and can be assigned to Cu^+ species in an oxide-like environment obviously located in the super cages. Thus, the results of CO adsorption reveal in contrast to the TPR results that the activation procedure leads to more available Cu^+ sites which are indispensable for the efficient fixation of CO for the OCM reaction.

3.2. Catalytic performance

The dependence of the MeOH conversion and product selectivities on the reaction temperature (130–170 °C) obtained for calcined and activated Cu-SAPO-37-ex under 0.4 MPa overall pressure are shown in Fig. 8(a) and (b), respectively.

It can be observed that the formation of DME is predominant on the calcined Cu-SAPO-37-ex sample (see Fig. 8a) pointing on the existence of acid sites catalyzing the etherification [36,37]. DMC and DMM are formed with low selectivity at low temperatures (130–150 °C) and almost disappeared at higher temperatures. The selectivity of MF is marginal. These findings indicate that during calcination at 550 °C a SSIE did not take place successfully, i.e. the distribution and fixation of Cu ions on acid sites of SAPO-37 are of minor extent, so that Cu species agglomerate and/or free acid sites still exist. FTIR spectra of pyridine adsorption (see Fig. 6 (spectra b)) confirm this, revealing the existence of the Lewis acid sites originated from agglomerated Cu as well as of portions of Brønsted acid sites on the calcined Cu-SAPO-37-ex sample.

In contrast, the formation of DMC (with a selectivity of 55–45%) and DMM (with a selectivity of ca. 40%) are predominant on the activated Cu-SAPO-37-ex (see Fig. 8b) at reaction temperatures of 130–170 °C. The methanol conversion is between 4% and 6%. Interestingly, the formation of DME and MF is negligible. This suggests an effective blocking of acid sites by Cu species originated from re-dispersion of larger Cu agglomerates. This conclusion can be supported by TPR and FTIR (see Fig. 6 (spectrum c)) results actually revealing a re-dispersion of a proportion of Cu after activation. This may lead, on the one side, to a diminution of both the Brønsted and Lewis acid sites. On the other side, such a re-dispersion may also create a co-existence of both the isolated and agglomerated Cu ions that was proposed to be required for DMC formation [38,39].

SAPO-37 belongs to the same FAU structure family like aluminosilicates X and Y, and the Cu modified variants of the latter have been already investigated for the OCM reaction [23,39,40]. Therefore, it is worth to compare the catalytic performance of the Cu-SAPO-37-ex sample with one of the Cu-containing Y zeolite samples in the OCM reaction. The properties of the latter were thoroughly studied recently in our lab by Richter et al. [23,30].

Fig. 9 depicts results of the catalytic measurements under normal pressure for the Cu-SAPO-5-ex and 16Cu-Y samples (this sample contains 16 wt.% Cu), both were activated in argon at 600 °C for 8 h before reaction. It can be seen that the conversion of MeOH as well as the selectivities for DMC and DMM on both the catalysts are more or less comparable in the temperature range from 120 to 220 °C. But, while the selectivity for DME on Cu-SAPO-37-ex remains almost unchanged in this temperature range, the one on 16Cu-Y drastically increases. This strongly suggests that the blockage of acid sites on SAPO-37 by Cu species should be different and may be more effectively than the one on Y zeolite. This suggestion may play an important role by investigating possible advantages in using Cu-SAPO-37 as catalyst and it is surely worth to be proved in the near future.

4. Conclusions

Copper can be successfully introduced into silicoaluminophosphate structure SAPO-37 by solid state ion exchange using Cu(II) acetyl acetonate powder. This strategy is applied for the first time to successfully synthesize Cu-SAPO-37 solids and it circumvents structural breakdown when using aqueous copper solutions for impregnation or ion exchange. The solid state ion exchange ran efficient when the template is extracted from the synthesis form of SAPO-37 by a treatment with methanolic HCl solution. The resulting Cu-SAPO-37-ex retains the FAU structure and, after appropriated activation, could be used as catalyst for the oxidative carbonylation of methanol (OCM) under pressure with a DMC selectivity of 55–45% at 130–170 °C. The differences between calcined and activated Cu-SAPO-37-ex can be explained by the favored auto-reduction of Cu^{2+} to Cu^+ accompanied by a re-dispersion of Cu species during the activation in inert gas. Future work will be concentrated on a variation in the copper source probably leading to improvements in final Cu-content and increased catalytic

activity of those samples. In addition, the further variation in reaction parameters such as residence time, reaction pressure and molar reactant ratio may positively affect the reaction outcome with respect to methanol conversion and DMC and DMM yield, respectively.

Acknowledgements

Thi Thuy Hanh Dang gratefully acknowledges grants from the Government of S. R. Vietnam, the DAAD and LIKAT. The authors thank Dr. M. Richter, Dr. H.-L. Zubowa, Mrs W. Winkler and Mr R. Eckelt (all of LIKAT) for their worthwhile contribution and cooperation.

References

[1] T. Sakakura, K. Kohno, Chemical Communications (2009) 1312–1330.
[2] M. Honda, S. Kuno, S. Sonehara, K.-i. Fujimoto, K. Suzuki, Y. Nakagawa, K. Tomishige, ChemCatChem 3 (2011) 365–370.
[3] W.-L. Dai, S.-L. Luo, S.-F. Yin, C.-T. Au, Applied Catalysis A – General 366 (2009) 2–12.
[4] D. Delledonne, F. Rivetti, U. Romano, Applied Catalysis A – General 221 (2001) 241–251.
[5] Z. Li, K. Xie, R.C.T. Slade, Applied Catalysis A – General 205 (2001) 85–92.
[6] M. Richter, M.J.G. Fait, R. Eckelt, E. Schreier, M. Schneider, M.M. Pohl, R. Fricke, Applied Catalysis B: Environmental 73 (2007) 269–281.
[7] L.B. McCusker, D.H. Olson, Atlas of Zeolite Framework Types, sixth edition, Elsevier Science B.V., Amsterdam, 2007, pp. 1–2.
[8] B.M. Lok, C.A. Messina, R.L. Patton, R.T. Gajek, T.R. Cannan, E.M. Flanigen, Journal of the American Chemical Society 106 (1984) 6092–6093.
[9] P.P. Man, M. Briend, M.J. Peltre, A. Lamy, P. Beaunier, D. Barthomeuf, Zeolites 11 (1991) 563–572.
[10] A.F. Ojo, J. Dwyer, J. Dewing, K. Karim, Journal of the Chemical Society, Faraday Transactions 87 (1991) 2679–2684.
[11] K.V.V.S.B.S.R.M.S.J. Kulkarni, R.R. Rao, M. Subrahmanyam, A.V.R. Rao, Indian Journal of Chemistry, Section A 35A (1996) 875–877.
[12] H.B. Mostad, M. Stöcker, A. Karlsson, T. Rørvik, Applied Catalysis A – General 144 (1996) 305–317.
[13] J.M. Lopes, F. Lemos, F.R. Ribeiro, E.G. Derouane, Studies in Surface Science and Catalysis 69 (1991) 365–372.
[14] J. Dwyer, J. Dewing, K. Karim, S. Holmes, A.F. Ojo, A.A. Garforth, D.J. Rawlence, Studies in Surface Science and Catalysis 69 (1991) 1–24.
[15] P.B. Malla, S. Komarneni, Zeolites 15 (1995) 324–332.
[16] C.W. Lee, X. Chen, M. Zamadics, L. Kevan, Journal of the Chemical Society, Faraday Transactions 89 (1993) 4137–4140.
[17] M. Zamadics, L. Kevan, Journal of Physical Chemistry 97 (1993) 10102–10107.
[18] E.I. Tsyganova, L.M. Dyagileva, Russian Chemical Reviews 65 (1996) 315–328.
[19] A.G. Nasibulin, E.I. Kauppinen, D.P. Brown, J.K. Jokiniemi, Journal of Physical Chemistry B 105 (2001) 11067–11075.
[20] A.G. Nasibulin, O. Richard, E.I. Kauppinen, D.P. Brown, J.K. Jokiniemi, I.S. Altman, Aerosol Science and Technology 36 (2002) 899–911.
[21] D.A.M. Monti, A. Baiker, Journal of Catalysis 83 (1983) 323–335.
[22] D.L. Hoang, H. Lieske, Thermochimica Acta 345 (2000) 93–99.
[23] M. Richter, M.J.G. Fait, R. Eckelt, M. Schneider, J. Radnik, D. Heidemann, R. Fricke, Journal of Catalysis 245 (2007) 11–24.
[24] T.T.H. Dang, Thesis, Universität Rostock, 2011.
[25] A. Buchholz, W. Wang, A. Arnold, M. Xu, M. Hunger, Microporous Mesoporous Materials 57 (2003) 157–168.
[26] D.L. Hoang, T.T.H. Dang, J. Engeldinger, M. Schneider, J. Radnik, M. Richter, A. Martin, Journal of Solid State Chemistry 184 (2011) 1915–1923.
[27] R. Buzzoni, S. Bordiga, G. Ricchiardi, C. Lamberti, A. Zecchina, G. Bellussi, Langmuir 12 (1996) 930–940.
[28] G. Busca, Physical Chemistry Chemical Physics 1 (1999) 723–736.
[29] J.A. Lercher, C. Gründling, G. Eder-Mirth, Catalysis Today 27 (1996) 353–376.
[30] J. Engeldinger, C. Domke, M. Richter, U. Bentrup, Applied Catalysis A – General 382 (2010) 303–311.
[31] A. Davydov, Molecular Spectroscopy of Oxide Catalyst Surfaces, John Wiley & Sons Ltd., 2003, pp. 559–641.
[32] J. Howard, J.M. Nicol, Zeolites 8 (1988) 142–150.
[33] G.T. Palomino, S. Bordiga, A. Zecchina, G.L. Marra, C. Lamberti, Journal of Physical Chemistry B 104 (2000) 8641–8651.
[34] A.A. Davydov, A.A. Budneva, Reaction Kinetics and Catalysis Letters 25 (1984) 121–124.
[35] B. Guido, Journal of Molecular Catalysis 43 (1987) 225–236.
[36] M. Xu, J.H. Lunsford, D.W. Goodman, A. Bhattacharyya, Applied Catalysis A – General 149 (1997) 289–301.
[37] F.S. Ramos, A.M.D. de Farias, L.E.P. Borges, J.L. Monteiro, M.A. Fraga, E.F. Sousa-Aguiar, L.G. Appel, Catalysis Today 101 (2005) 39–44.
[38] S.T. King, Catalysis Today 33 (1997) 173–182.
[39] S.A. Anderson, T.W. Root, Journal of Catalysis 217 (2003) 396–405.
[40] S.A. Anderson, T.W. Root, Journal of Molecular Catalysis A: Chemical 220 (2004) 247–255.